Stable aqueous dispersions of carbon nanohorns loaded with minocycline and exhibiting antibacterial activity

Maeda Yukari[1], Hirata Eri[1*], Takano Yuta[2,3*], Sakaguchi Norihito[4], Ushijima Natsumi[5], Saeki Ayumi[6], Kimura Sadahito[1], Shibata Ken-ichiro[6], Yudasaka Masako[7,8], Yokoyama Atsuro[1]

[1] Oral Functional Prosthodontics, Division of Oral Functional Science, Faculty of Dental Medicine, Hokkaido University, Sapporo 060-8586, Japan

[2] Research Institute for Electronic Science and Graduate School of Environmental Science, Hokkaido University, Kita20, Nishi10, Sapporo 001-0020, Japan

[3] Graduate School of Environmental Science, Hokkaido University, Kita10, Nishi5, Sapporo 060-0810, Japan.

[4] Center for Advanced Research of Energy and Materials, Faculty of Engineering, Hokkaido University, Kita13 Nishi8, Sapporo 060-8628, Japan

[5] Support Section for Education and Research, Faculty of Dental Medicine, Hokkaido University, Sapporo 060-8586, Japan

[6] Division of Oral Molecular Microbiology, Department of Oral Pathobiological Science, Graduate School of Dental Medicine, Hokkaido University, Sapporo 060-8586, Japan

[7] Nanomaterials Research Institute (NMRI), National Institute of Advanced Industrial Science and Technology (AIST), Tsukuba Central 5, 1-1-1 Higashi, Tsukuba, Ibaraki 305-8565, Japan

[8] Meijo University, Graduate School of Science and Technology 1-501, Shiogamaguchi, Tenpaku, Nagoya 468-8502, Japan.

*Corresponding author:

Eri Hirata, Email: erieri@den.hokudai.ac.jp; Tel: +81 11706 4270,

Yuta Takano Email: tak@es.hokudai.ac.jp

Abstract

This work demonstrates that certain medically-approved drugs possess dual functions such that they exhibit intrinsic drug effects and can assist in dispersing carbon nanomaterials. Two types of carbon nanohorns (CNHs) (unoxidized: as-CNH, oxidized: CNHox550) and carbon nanotubes (CNTs) were successfully dispersed in aqueous solutions using minocycline (MC) as a dispersant. Absorption spectra, thermogravimetric analyses and theoretical calculations demonstrated that the MC was attached to the CNHs in these dispersions. The antibacterial activities of these MC/CNH complexes were examined using *Streptcoccus mutans* and *Aggregatibacter actinomycetemcomitans*, and the MC/as-CNH complex was found to maintain the same bacterial growth inhibition activity as the original MC. Electron microscopy observations suggested direct contact of the MC/CNH complexes with the bacteria, presumably allowing delivery of the MC. The results obtained from our study demonstrate that drug/nanocarbon complexes have potential applications in drug delivery.

1. Introduction

The unique characteristics of carbon nanomaterials (CNMs), including graphene, carbon nanotubes (CNTs) and carbon nanohorns (CNHs), make these ideal candidates for biomedical applications such as regenerative therapy, immunotherapy, gene therapy and cancer treatment [1–9]. In such biomedical applications, the dispersion of CNMs in water is often required to combine these substances with water-soluble biomolecules, proteins, drugs or scaffolds such as collagen gels or hydrogels [10][11]. Thus, amphiphilic surfactants or chemical modifications are applied to confer water solubility [12][13]. Although sodium dodecyl sulfate (SDS), sodium dodecyl benzene sulfate (SDBS), steroidal surfactants such as sodium cholate (SC), sodium deoxycholate (DOC) and polyethylene glycol are often used to disperse CNMs, these may disrupt cellular activities, can be cytotoxic and can also inhibit the effect of drugs loaded onto the CNMs. Alternatively, chemical modifications, such as the introduction of carboxylic groups, hydroxyl groups or polyethylene glycol chains, can be applied to disperse CNMs, although these modifications may change the physical properties and biological activity of the CNMs [10][11]. Therefore, it would be helpful to identify better dispersion methods for CNMs than those reported previously. However, no medically-approved drugs are known to act as surfactants while exhibiting intrinsic medicinal activity, even though the use of such compounds could mitigate the issues described above by removing the need to add surfactants.

Among the various CNMs, CNHs have attracted significant interest with regard to biomedical applications because of their unique structures, comprising tubules with horn-shaped tips that are 2-5 nm in diameter and 40-50 nm in length. In these materials, thousands of such tubules assemble to form spherical aggregates with diameters of approximately 100 nm [14]. These substances have been reported to exhibit significant biocompatibility [15–17] because their preparation does not involve metal catalysts [18]. CNHs are also approximately isotropic in three dimensions owing to their spherical morphology, which may be another reason for their low toxicity [19]. Previously, we reported that CNHs enhance osteogenesis [20] and, when integrated with macrophages, increase osteoblast differentiation [21]. CNHs also have the potential to act as carriers for various drugs [22].

Minocycline (MC) is one of the most widely used medically approved antibiotics [23] and often used for inflammation of the maxillofacial region, especially the jawbone. By intravenous injection or internal administration, only a small amount of the drug reaches the local area. Therefore, local administration of MC to the inflammation site is effective. In this context, we anticipated that CNHs could serve as carriers for local drug delivery carrier of MC. It has been reported that the nanohorn tubules, which are initially closed, can be opened by oxidation, such that the specific surface area of oxidized CNHs (termed CNHox550 in our work) is twice that of unoxidized material (as-CNH) [24][25]. This increased surface area is beneficial when loading the nanohorns with drugs such as cisplatin or vancomycin [26][22]. However, the poor dispersion of CNHs in water as a result of the intrinsic hydrophobicity of these materials remains a challenge. The present study demonstrates that MC acts as a good dispersion agent for both CNHs and CNTs. Moreover, the complex formed by combining MC and as-CNHs exhibits the same anti-bacteriostatic properties as MC. This effect is demonstrated in the present work in trials using adherent cells comprising an osteoblastic cell line.

2. Materials & Methods

2.1 General

Minocycline hydrochloride (MC) and organic solvents were purchased from Fuji Film Wako Corporation (Japan), while CNHs were obtained from NEC Corporation (Tokyo, Japan). These materials were produced by the ablation of a pure graphite target at room temperature in Ar at 760 Torr using a CO_2 laser [27]. The CNHs were approximately 95% pure, with the majority of the impurities consisting of graphitic spheres [28]. No metal catalyst was used in the preparation of these samples. Air-oxidized CNHs were prepared using a previously reported procedure. In this process, the CNHs were heated under a flow of air while applying a temperature increase rate of 1 °C/min to a final temperature of 550 °C, then cooled under an air flow [29]. Single walled carbon nanotubes (SWCNTs) were purchased from the ILJIN NANOTECH Company (Seoul, South Korea) and used after oxidation by immersion in an aqueous H_2O_2 solution at approximately 70 °C. This process enhanced their hydrophilicity by increasing the concentration of surface oxygen-containing functional groups.

2.2 Preparation of MC/CNH complexes

MC (1.0 mg) was dissolved in 10 mL of deionized water to prepare a stock solution. MC/CNH complexes were prepared by adding 1.0 mg of as-grown CNHs (as-CNHs) or CNHs oxidized at 550 °C (CNHox550) to 10 mL of an MC solution. The resulting mixture was subsequently sonicated at a temperature of 5 to 10 °C for 2 h. The MC solutions used in these trials had concentrations of 0, 20, 40, 60, 80, 100 or 150 μg/mL, while the CNH concentration was held constant at 100 μg/mL. In experiments using bacterial or cell cultures, the dispersion was added to the culture medium at the concentrations described below.

2.3 Preparation of MC/SWCNT complexes

Mixtures were prepared by adding 0.33 mL of an aqueous dispersion of SWCNTs (3.0 mg/ml) to 10 mL of an aqueous solution of MC (0.12 mg/mL). Each mixture was then subjected to sonication in ice water for approximately 4 h (similar to the treatment of the CNH specimens) to produce an MC/SWCNT dispersion.

2.4 Theoretical calculations

Geometries were optimized using the Gaussian 09 program (Revision D.01) [30] with the B3LYP [31][32][33] functional and the D3 version of Grimme's dispersion with the original D3 damping function [34]. The 6-31G(d) [35,36] basis set was used for H, C, N and O atoms. The basis set superposition errors (BSSEs) were evaluated using the counterpoise method in the Gaussian 09 package.

2.5 Transmission electron microscopy observations of MC/CNH samples

Immediately after synthesis, MC/CNH samples were observed using high-resolution transmission electron microscopy (HR-TEM; JEM-2010F, JEOL, Tokyo, Japan), operating at an acceleration voltage of 200 kV. Specimens were also examined using high-angle annular dark field scanning TEM (HAADF-STEM; Titan-cubed G2 60-300, FEI, Hillsboro, USA) at an acceleration voltage of 80 kV. For comparison purposes, CNHs dispersed in 100% ethanol were also observed.

2.6 Absorption spectroscopy

To estimate the dispersion of the MC/CNH samples, the absorbance of dispersions of CNHs and MC/CNH samples were determined at 600 nm using a Nanodrop UV–vis spectrophotometer (Thermo™INSIGHT, ThermoFischer, Waltham, USA).

2.7 Thermogravimetric analysis

Prior to thermogravimetric analysis (TGA), the MC/CNH dispersions were lyophilized using a VD-400F instrument (TAITEC, Saitama, Japan) to obtain black powders. TGA was carried out with a TG 8120 instrument (Rigaku Corporation, Tokyo, Japan). In each trial, a 2 mg sample was placed on a platinum pan and the sample temperature was increased from ambient to 900 °C at a rate of 10 °C/min under a 100 mL/min N_2 flow.

2.8 Quantification of released MC

The amount of MC released from each MC/CNH specimen was quantified using dialysis cassettes (Slide-A-Lyzer G2, MWCO 7k Da, ThermoFischer, Waltham, USA). In each trial, a 0.5 mL aliquot of the MC/CNH suspension was transferred to a dialysis cassette (volume range 0.25-0.5 mL) that was

subsequently placed in 10 mL of a phosphate buffer solution (PBS; Wako, Osaka, Japan) at room temperature. A 100 μL portion of the suspension was taken from the exterior solution of the dialysis cassette at intervals of 1, 2, 5 and 8 h and 1, 2, 3 and 7 days. The absorbance of each sample at 350 nm was assessed using the UV–vis spectrophotometer described above.

2.9 Bacterial culture

Streptcoccus mutans (*S.m.*) (ATCC 55677) was cultured in a brain heart infusion (BHI; BD, Franklin Lakes, USA) medium and *Aggregatibacter actinomycetemcomitans* (*A.a.*) (ATCC 29522) was cultured in a BHI medium with 1% yeast (Bacto™ Yeast Extract; BD, Franklin Lakes, USA). The MC/CNH dispersion solution was added to each culture medium to give MC concentrations of 0, 0.05, 0.1, 0.2, 0.4 or 0.8 μg/mL. The tube containing the culture medium was subsequently incubated at 37 °C in an atmosphere comprising air containing 5% CO_2. After 24 h, the absorbance at 600 nm was determined using a SmartSpec Plus instrument (BIO-RAD, Hercules, USA), and this value was taken to indicate the turbidity of the medium. The growth rate in the culture was estimated from the ratio of the absorbance values obtained at 24 and 0 h (meaning the point at which the bacteria were seeded).

2.10 TEM observations of bacteria

After each specimen was cultured for 20 h, the bacteria were observed by TEM (JEM1400, 80 V, JEOL, Tokyo, Japan). The bacteria were fixed with 2% glutaraldehyde. For TEM observations, specimens were stained with 1% OsO_4 and embedded in epoxy resin after dehydration. Ultrathin sections were obtained using an ultramicrotome (Leica, Wetzlar, Germany) with a diamond knife (DiATOME, Nidau, Switzerland), and subsequently examined using TEM.

2.11 Osteoblast cell cultures

Mouse osteoblast MC3T3-E1 cells were suspended in a general medium at a concentration of 6.67×10^4 cells/mL in minimum essential medium alpha modification (α-MEM; Gibco, ThermoFischer, Waltham, USA), containing 5% fetal bovine serum (FBS; Biowest, Nuaillé, France), 100 units/mL penicillin, 100 μg/mL streptomycin, (Pen Strep; Gibco, France) and 5 μL/mL L-glutamine (Sigma-Aldrich, St. Louis, USA). In each case, 300 μL of the cell suspension was seeded into each well of a 48 well plate.

After 3 h, the culture medium was replaced with an osteoblast differentiation medium consisting of 50 µM ascorbic acid and 10 mM β-glycerophosphate together with MC/as-CNH or MC/CNHox550 dispersions at a concentration equivalent to 0.8 µg/mL MC. After a 7 d cell culture, the DNA concentration and alkaline phosphatase (ALP) activity of each sample were measured. Prior to this process, each well was washed twice with PBS and 300 µL of a cell suspension containing 0.2% IGEPAL CA630 (Sigma-Aldrich, St. Louis, USA), 10 mM tris-HCl and 1 mM $MgCl_2$ (pH 7.4) was added to each sample. The samples were subsequently frozen, thawed and homogenized, and each sample solution was added to 100 mL of 4 M NaCl in a 0.1 M phosphate buffer (pH 7.4) and then centrifuged for DNA analysis. Picogreen (Molecular Probes, Leiden, Netherlands) was used to determine the DNA content in conjunction with a microplate reader (infinite F200 PRO, TECAN, Kanagawa, Japan) with the excitation filter set at 365 nm and the emission filter at 450 nm. The ALP activity was found using a LabAssay apparatus (Wako, Osaka, Japan) following a procedure previously described in the literature [21]. The resulting ALP activity values were normalized relative to the DNA concentration. The DNA level and ALP activity were determined for five samples, and all values are presented herein together with the standard error of the mean (SEM). Statistical analyses were performed using the GraphPad Prism software package (GraphPad, San Diego, USA), applying a one-way ANOVA based on Dunn's multiple comparisons test.

3. Results and Discussion

3.1 Preparation and characterization of MC/CNH complexes

The dispersions of CNH with MC were prepared from solutions in which the concentration of MC was kept constant at 0, 20, 40, 60, 80, 100, or 150 μg/mL (these values are hereinafter used to describe the dispersions) and the concentration of CNH was kept constant at 100 μg/mL. The MC/as-CNH dispersions (Figure 1A(b)) were found to be stable for longer than 24 h, whereas the as-CNH materials dispersed without MC (Figure 1A(a)) were observed to precipitate over this time span. The CNHox550 remained dispersed in water both with and without MC (Figures 1A(c) and 1A(d)) because it has the numerous oxygen-containing groups such as carboxyl and carbonyl carboxylic groups [28] [29] [37]. Surprisingly, absorbance of the as-CNH at 600 nm, at which wavelength the MC does not absorb, was increased by a factor of 1.7 upon adding MC at 100 μg/mL (Figure 1B), confirming that the dispersion of this material was improved by the presence of the MC.

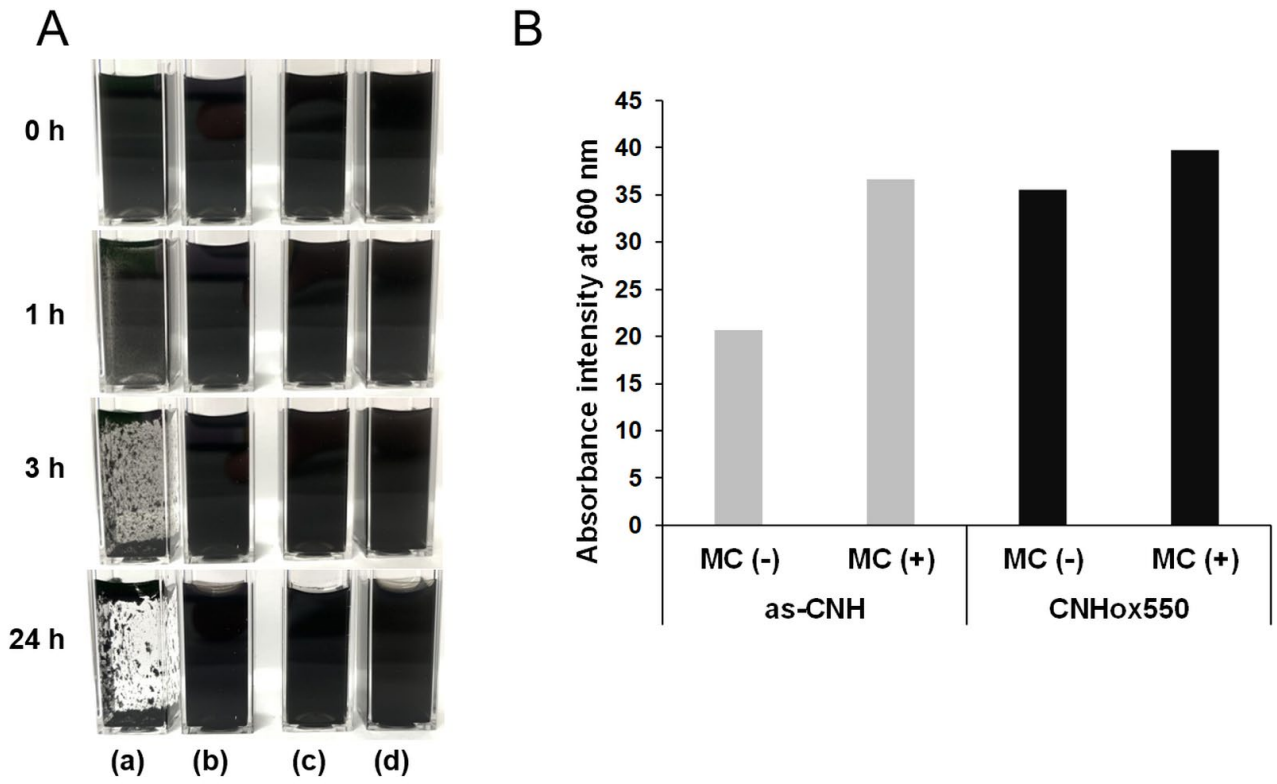

Fig. 1 (A) Photographic images of suspensions of (a) as-CNH, (b) MC/as-CNH, (c) CNHox550 and (d) MC/CNHox550 specimens acquired 0, 1, 3 and 24 h after 2 h sonication. (B) Absorbance at 600 nm after addition of 100 μg/mL MC and sonication, to evaluate the dispersion of CNHs.

Typically, CNHs require the addition of dispersants or the application of chemical modifications to obtain stable suspensions in aqueous media [22]. Even so, the present study confirmed, for the first time, that MC promotes the dispersion of CNHs in water. It was also found that as-CNHs could be dispersed in even PBS with the support of MC (Figure S1). Furthermore, this work confirmed that MC can disperse CNTs (Figure S2), indicating the potential versatility of the present method with regard to generating stable suspension of various other CNMs.

Density functional theory (DFT) calculations were performed to confirm the feasibility of attaching MC molecules to CNM surfaces. The focus was on binding energies, which represent intermolecular interactions between two molecules. These were used to examine the degree of interaction between various drug molecules and the CNMs [38]. A graphene sheet was modeled during these calculations as a representation of the flat surface of a CNM and (10,0) CNTs were used to model a typical curved graphene-like structure (Figures S3 and S4).

Camptothecin was employed to provide a basis for comparison with the results for MC. Camptothecin is a hydrophobic molecule that can attach to CNTs via π-π and van der Waals interactions [39]. The B3LYP-D3/6-31G level of theory was used to calculate dispersion forces when estimating intermolecular π-π interactions [30][34]. The results indicated that MC interacts strongly with graphene structures comparable to those of camptothecin (Table 1), which may be due to the intermolecular interactions.

Table 1. Binding energies (Δ*E*) for the complexes.[a]

(a) Energies calculated at the B3LYP-D3/6-31G(d) levels with BSSE correction by the counterpoise method, using geometries optimized at the B3LYP-D3/6-31G(d) level.

	ΔE (kcal mol^{-1})
MC/graphene	–32.3
camptothecin /graphene	–33.2
MC/SWNTs	-27.2
camptothecin /SWNTs	–23.3

The interactions of MC are also strong when this molecule is combined with the curved structures of a CNT, which can occur in CNHs. The DFT calculations predict the higher binding energy of the MC/CNT complex as compared to that of the camptothecin/CNT combination. This result implies that the interactions of MC are stronger, perhaps because the shape of the MC fits the curvature of CNT, based on the similarity in the intermolecular interaction. These data indicate that the π-conjugated structure and curved morphology of the MC allow this compound to attach to CNMs. In addition, the hydrophilic portions of the MC molecule render the complex water-soluble, such that the MC can act as an amphiphilic surfactant.

Figure 2A presents the absorbance spectra of dispersions of MC, as-CNH and MC/as-CNH. The first two spectra exhibit a characteristic peak due to MC at approximately 345 nm. In addition, the CNHs show a gradual increase in absorbance as the wavelength decreases from 800 to 300 nm. To better assess the MC absorbance peak at 345 nm, the CNH spectrum was subtracted from the MC/CNH spectra after adjusting the CNH spectrum so that the absorbance between 600 and 700 nm was nil (Figures 2B and C). Following this manipulation, it is evident that the MC peak intensity increased along with the MC concentration (see Figure 2D). Since free MC molecules were not removed from the MC-CNH dispersions, the MC peaks at 345 nm in the MC/CNH spectra can be assigned to these free MC molecules as well as those attached to the CNHs. However, the absorbance of MC attached to the CNHs could be weaker than that of free MC due to the strong electronic interactions between the MC and CNHs (similar to the case of phthalocyanine attached to CNHs [40]). Therefore, the reduced absorbance at 345 nm exhibited by the MC/CNHox550 dispersion as compared to that of the

pure MC solution (Figure 2D) indicates that a certain amount of the MC was firmly attached to the CNHs. This might reflect the greater surface area of the CNHox550, in which holes were opened by oxidation such that it had approximately twice the surface area of the as-CNH [41]. There is a specific threshold concentration to become indicative of MC absorbance, which varies between MC/as-CNH (0 to 20 μg/mL) and MC/CNHox550 (40 to 60 μg/mL). The reason for the appearance of the threshold concentration is not clear, but we propose that a certain amount of the MC was encapsulated inside the CNHox550, such that the MC did not absorb light to the same extent.

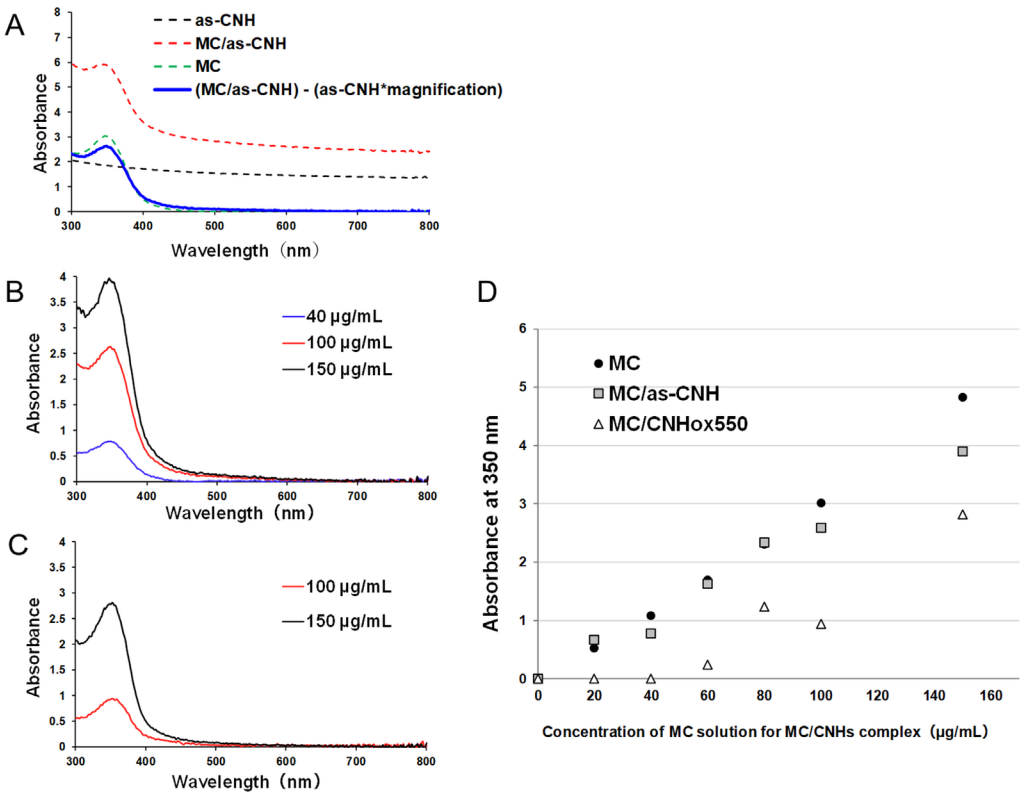

Fig. 2. (A) Absorbance spectra of dispersions of MC (100 μg/mL; green dashed line), as-CNHs (100 μg/mL; black dashed line) and MC/as-CNH (MC, as-CNHs = 100 μg/mL; red dashed line). The absorbance spectrum of MC in the MC/as-CNH dispersion (blue solid line) was extracted by subtracting the CNH spectrum from the MC/CNH spectrum after adjusting the CNH spectrum so that the absorbance between 600 and 700 nm was nil. Extracted absorbance spectra of MC in (B) MC/as-CNH and (C) MC/CNHox550 dispersions. The spectra exhibit a characteristic peak for MC. (D). Absorbance values at 350 nm as a function of MC concentration in an aqueous solution of MC, the solutions in Fig 2B, and Fig 2C. The absorbance shows the detectable amount of MC by the spectrometer. The CNH concentration was 100 μg/mL in each case.

TGA was performed in a N_2 atmosphere to examine the attachment of MC to the as-CNH and CNHox550. The pure MC showed a mass loss from at 230 °C, followed by monotonous and continuous loss, assigned to vaporization or decomposition of MC, with a final mass loss of 75% at 900 °C (Figure 3C). 25% of the residue is non-gasified and high-carbide of pyrolysis MC. The pure as-CNHs and CNHox550 did not exhibit any mass loss around 230 °C and their mass losses at 900 °C were 40% and 26%, respectively (Figures 3A and B). The MC/as-CNHs and MC/CNHox550 complexes showed mass losses beginning at 230 °C (Figures 3D and E) and a residue at 900 °C. These results, however, are not readily explained. Because the samples were prepared by mixing equal masses of MC and as-CNH or CNHox550, the theoretical mass losses at 900 °C would be approximately 57% (=(75+40)/2) and 50% (=(75+26)/2) for the MC/as-CNH and MC/CNHox550, respectively. The latter produced the expected mass loss of about 50% (Figure 3E) but the former did not (about 85%; Figure 3D). It is likely that the size of the MC particles and the sites on which they were adsorbed could have had an effect. The MC agglomerates in the MC/as-CNH were likely small as a result of the nanometer-sized deposition sites on the as-CNH surface, resulting in rapid evaporation at 230 °C and the following continuous mass loss up to 900 °C. A weight loss was observed at about 500 ºC for MC/as-CNHs (Figure 3D) which may be due to the MC absorbing more strongly on as-CNHs for some reason. For MC/CNHox550, certain amounts of the MC were confined inside the nanospaces of the CNH tubules. MC therefore did not evaporate readily such that they remained as a highly-carbonized residue at 900 °C. In contrast, the MC used for the TGA trials was a powder having a smaller surface area, which could explain the mass loss similar to that of the MC in the MC/as-CNH.

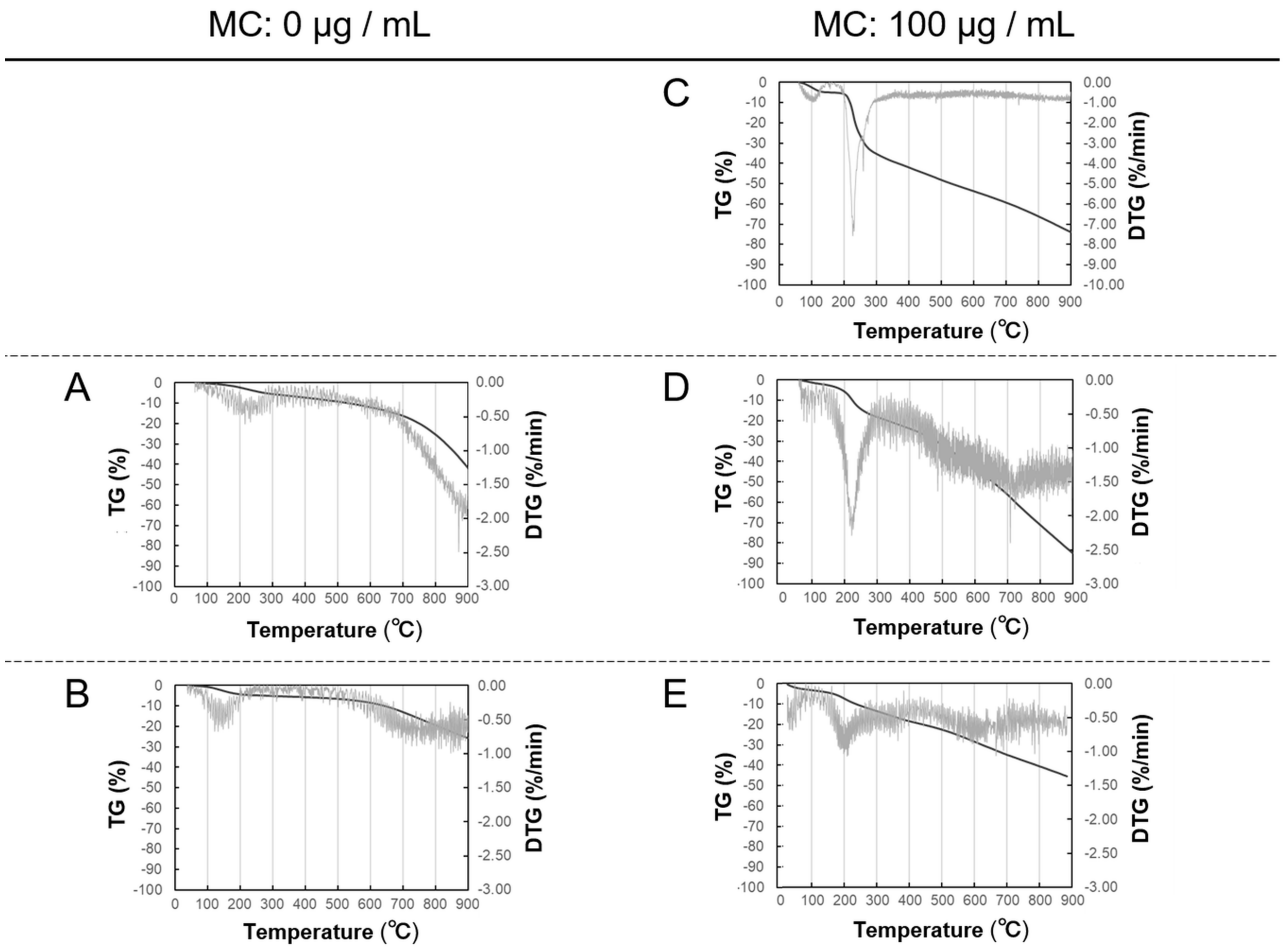

Fig. 3 Thermogravimetric (TG) and differential TG (DTG) data for (A) as-CNH, (B) CNHox550, (C) MC alone, (D) MC/as-CNH and (E) MC/CNHox550 specimens. The concentration of MC in the original dispersion was nil (A, B) and 100 mg/mL (C-E), while the concentration of CNH was kept constant at 100 μg/mL (A, B, D, E).

TEM observations of the MC/CNH samples were also performed and Figures 4A and 4B-D show the as-CNH and MC/as-CNH images, respectively. Figure 4E presents the CNHox550 image while Figure 4F-H shows the MC/CNHox550. In Figure 4E, well-defined holes at the tips of the horns are evident, as indicated by the white arrowhead. Figures 4B and 4F demonstrate many deposits around the horn structures, some of which may have been MC. Despite the close observations by HR-TEM at a low acceleration voltage of 80 kV and examinations by STEM, it is difficult to conclusively identify MC molecules due to the low contrast and to thermal changes in the positions and molecular configurations of these molecules.

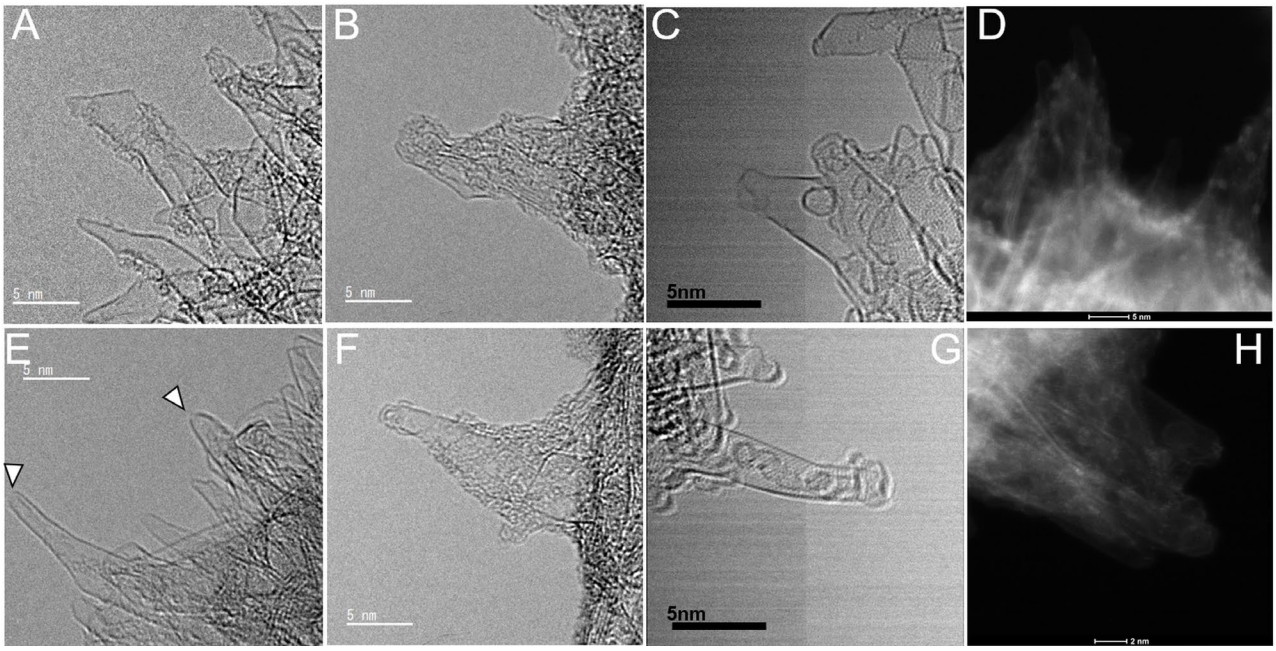

Fig. 4 TEM images of (A) as-CNH (HR-TEM 200 kV), (B) MC/as-CNH (HR-TEM 200 kV), (C) MC/as-CNH (HR-TEM 80 kV), (D) MC/as-CNH (HAADF-STEM 80 kV), (E) CNHox550 (HR-TEM 200 kV), (F) MC/CNHox550 (HR-TEM 200 kV), (G) MC/CNHox550 (HR-TEM 80 kV) and (H) MC/CNHox550 (HAADF-STEM 80 kV). The white arrows in E indicate holes in the horns.

3.2 Sustained release of MC

Before examining the antibiotic activity of the MC/CNHs, the feasibility of discriminating between free MC and MC attached to CNHs was examined, along with the abilities of the MC/CNH specimens to release MC. This was performed via a dialysis method in PBS. Absorbance spectra were acquired from the external PBS solutions obtained from the dialysis cassettes, and the amounts of MC detached from the MC/CNH specimens as well as the free MC were estimated from the optical absorbance at 350 nm. A control experiment was also performed using pure MC (Figure 5). The proportions of the optical absorbance at 350 nm after 1 d relative to that after 7 d were 71% for the MC/as-CNH and 55% for the MC/CNHox550. The MC alone exhibited rapid elution from the dialysis tube and almost complete elution within 24 h, such that 95% was removed after 7 d. The MC/as-CNH released 62% of the MC relative to the MC alone, whereas the MC/CNHox550 released 22% of the MC after 7 d of dialysis. These results suggest that the amount of MC that was easily dialyzed in the MC/as-CNH was

greater than that in the MC/CNHox550, or that the quantity of strongly-attached MC in the MC/CNHox550 was larger than that in the MC/as-CNH.

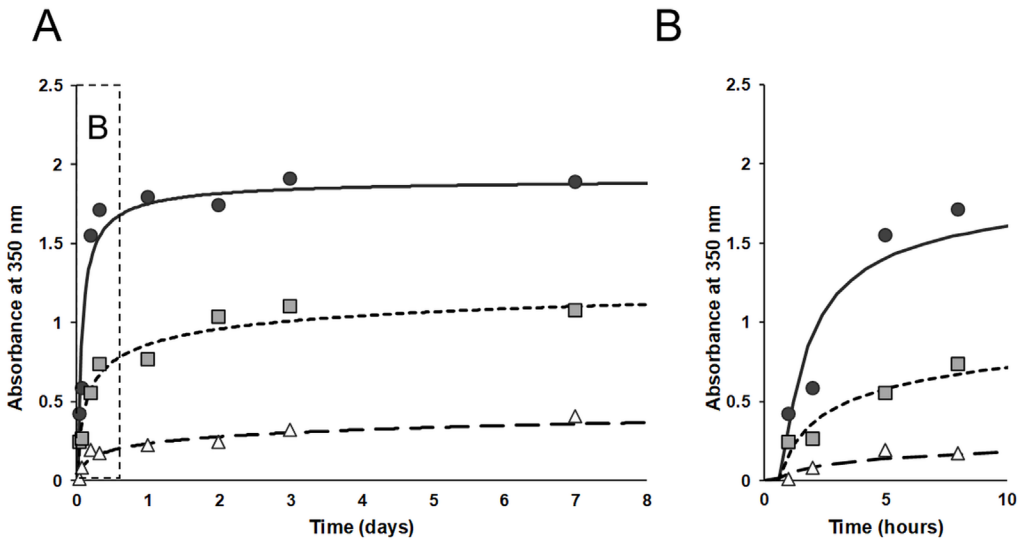

Fig. 5 (A) Time courses of MC release as determined by the intensity of the MC absorbance at 350 nm in 10 mL PBS dialysis solutions of MC alone (●), MC/as-CNH (■) and MC/CNHox550 (△). In each trial, 0.5 mL of the aqueous dispersion was added to the dialysis cassette and the concentrations of MC, as-CNH and CNHox550 in the initial dispersions were 0.1 mg/mL. (B) X axis-expanded profiles of Fig. 5A.

3.3 Bacterial culture

Figure 6 shows the growth rates of the *A.a.* (Figure 6A) and *S.m*. (Figure 6B) and demonstrates that MC concentrations of 0.1 μg/mL or higher showed a bacteriostatic effect against *A.a.* MC/as-CNH suppressed bacterial growth at the same concentration of MC alone. MC/CNHox550 at concentrations below 0.4 μg/mL had no effect. Similarly, MC alone or in the presence of MC/as-CNH at concentrations greater than 0.4 μg/mL inhibited the growth of S.m. MC/CNHox550 at concentrations greater than 0.8 μg/mL showed a bacteriostatic effect. Therefore the MC alone and MC/as-CNH evidently possessed comparable bacteriostatic effects, which was inconsistent with the results of the dialysis experiments showing that the amount of MC released from the MC/as-CNH was comparable to that for MC alone (Figure 5). The quantity of MC released from the MC/CNHox550 was smaller, about 15% of that from the MC alone (Figure 5), and so its antibacterial function was weaker (Figure

6).

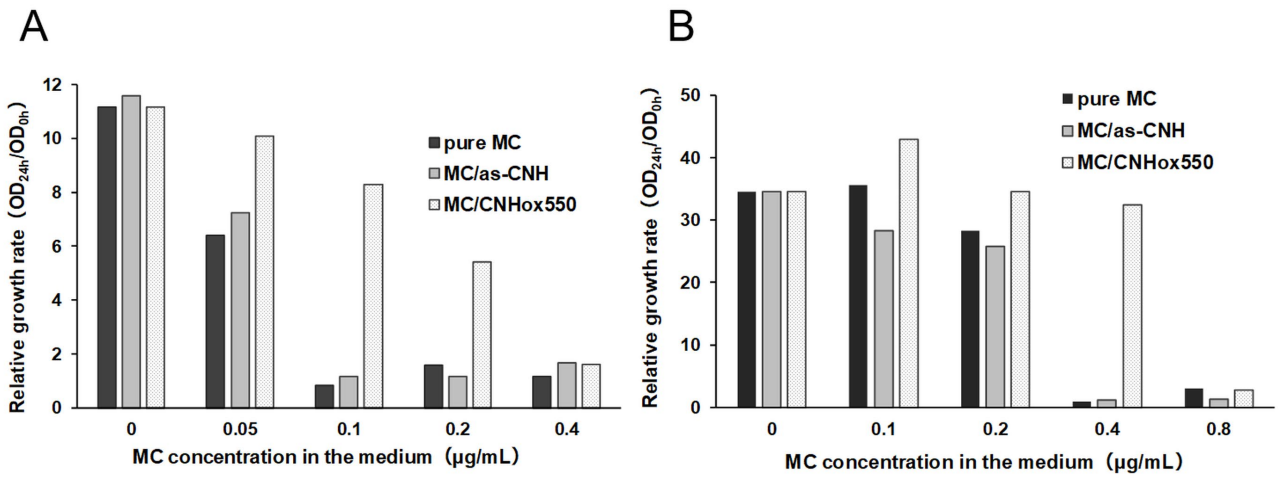

Fig. 6 Bacterial activities against (A) *A.a.* and (B) *S.m.* based on turbidity as reflected by absorbance at 600 nm. MC concentrations were 0, 0.05, 0.1, 0.2, 0.4 and 0.8 μg/mL. The growth rate was determined by ratioing the absorbance values at 24 h and 0 h.

Figure 7 shows TEM images after *A.a.* culturing in the medium (Figure 7A), with MC (Figure 7B), with as-CNH (Figure 7C), and with MC/as-CNH (Figure7D). MC exhibits bacteriostasis that inhibits the protein synthesis and biological activities of bacteria. Compared to the live *A.a.* (black arrow) in Figure 7A, the cell walls are thinner in the presence of MC in Figure 7B. Moreover, the cytoplasm (white arrowhead) is completely absent. In Figure 7C, the structure (black arrow) is unchanged for as-CNH (white arrow). However, as seen in Figure 7D for MC/as-CNH (gray arrow), there are cases of complete destruction of the cytoplasm (white arrowheads) and thinning of the cell walls. Therefore MC/as-CNHs can affect the bacteria via bacteriostasis of the MC on MC/as-CNHs.

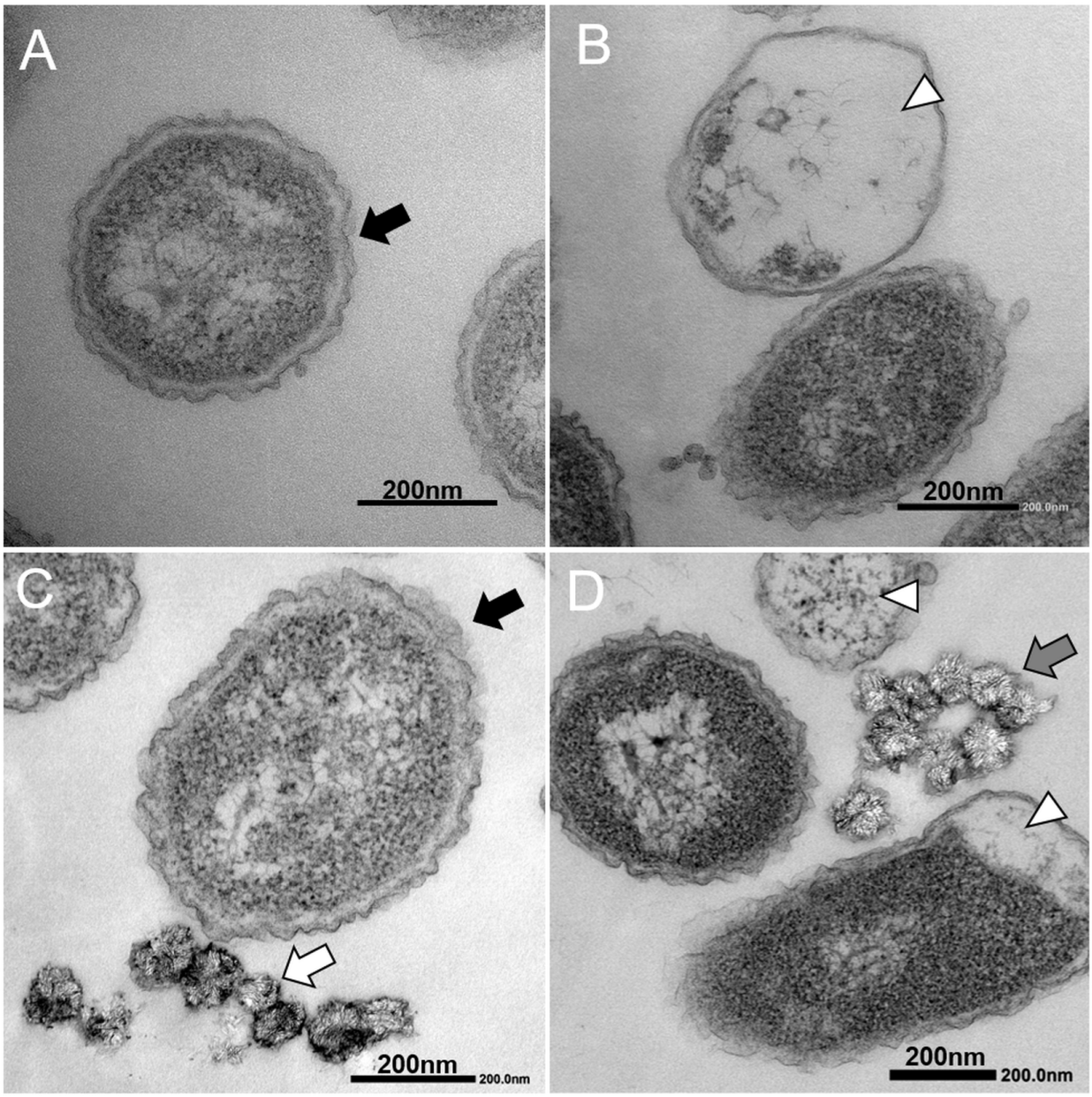

Fig. 7 TEM observation after *A.a.* culturing in the medium (A), with MC (B), with as-CNH (C), and with MC/as-CNH (D). Black arrows: live *A.a.*, white arrow: As-CNHs, gray arrow: MC/as-CNHs, white arrowheads: cytoplasm of *A.a.*

3.4. Osteoblast proliferation and differentiation

MC is frequently prescribed as local administration for inflammation in jawbone. To apply MC/CNHs for local drug delivery against inflammation, it is necessary to confirm that MC/CNHs do not harm bone tissue. In the present study, the effect of this material on the initial differentiation and proliferation of osteoblasts was examined by monitoring ALP activity, which is an early marker of

osteoblastic cell differentiation [37]. The DNA contents and ALP activities of cells cultivated for 7 d are shown in Figure 8.

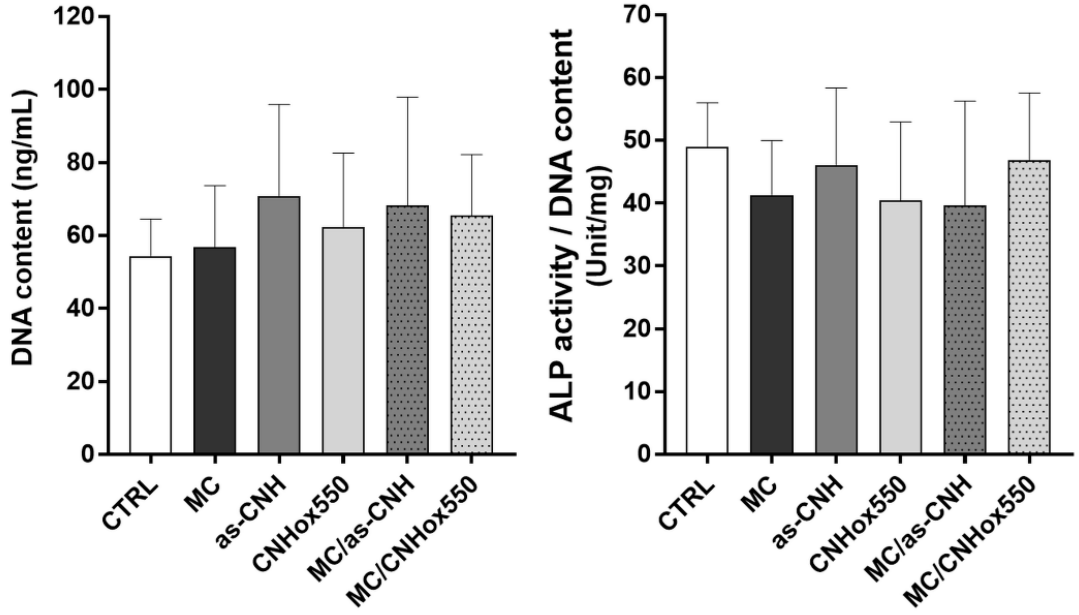

Fig. 8 DNA concentrations (left) and ALP activities normalized to DNA content (right) for the MC3T3-E1 cells cultured for 7 d (n = 6). There were no significant differences between each sample. Concentration: as-CNH = 0.8 μg/mL, CNHox550 = 0.8 μg/mL, MC = 0.8 μg/mL.

Compared to the absence of MC and CNHs as control trials, the DNA concentrations and ALP activities normalized relative to the DNA contents for the MC, as-CNHs, CNHox550, MC/as-CNH and MC/CNHox550 samples showed no significant differences ($p > 0.1$). There were also no significant differences between the "with MC" and the "with CNHs" groups. Thus, the presence of the MC/CNH and MC (which showed antibacterial effects) did not affect the cell differentiation and proliferation. This result is consistent with a report by Park et al. that only high concentrations of MC hydrochloride (more than 49.4 μg/mL or 100 μM) lead to a dose-dependent decrease in cellular differentiation and protein expression [42]. The presence of CNHs also had no negative effect on osteoblasts. This result is in agreement with our previous study indicating that the ALP activity of human mesenchymal stem

cells was not affected by CNHs [21]. Several researchers have also found that CNHs exhibit low toxicity. Based on *in vivo* toxicological assessments of CNHs, Miyawaki et al. reported that these materials were not irritants or dermal sensitizers, using primary and conjunctival discomfort tests and skin sensitization examinations. Intratracheal instillation tests revealed that, over a 90 d test period, SWNHs rarely weakened rat lung tissue, although black pigmentation was observed due to accumulated CNHs [17]. In addition, our own group has found that CNHs have high compatibility with bone tissue [20]. Several studies have examined the distribution of CNHs in mice because biodistribution is an important aspect of *in vivo* behavior when evaluating the biosafety of nanomaterials. Tahara et al. reported that the distribution of intravenously administered CNHs was affected by chemical functionalization and that CNH accumulation in the lungs decreased with increased hydrophilicity [43]. Zang et al. also assessed the biodistribution and excretion of CNHs in mice. CNHs were found to accumulate mainly in the liver and spleen, and a small amount of CNHs was excreted within the first few hours after injection, followed by much slower excretion rates after 48 h [44].

Previously, we have examined the distribution of SWCNTs based on near-infrared fluorescence imaging after implantation between the periosteum and parietal bone of mice [45]. Fluorescence was not observed in other organs, including the liver, spleen and lungs, in whole-body imaging experiments, whereas fluorescence was clearly observed in the cranial region even after 56 d. We suggested that locally implanted SWCNTs remain at the site of implantation and do not accumulate in detectable quantities in other organs. For biological applications, it is necessary to investigate biological reactions over long time spans, but the above reports establish the low toxicity of CNHs and SWNTs, thus we presume that the effects of MC/CNHs on osteoblasts and other systems in living organisms should be relatively minimal.

4. Conclusion

The present study verified that a medically approved drug, MC, can act as a suitable dispersant for nanocarbon materials such as CNHs and SWNTs, to promote their dispersion in water. The MC was found to adhere to CNHs at hydrophobic sites, while the hydrophilic parts of the MC molecules allowed the MC/CNH complexes to be dispersed in water. MC/as-CNH specimens also showed bacteriostatic properties comparable to that of the original MC. The use of MC as a dispersant for nanocarbon materials is beneficial because this removes the requirement to add additional surfactants that may perturb intrinsic cellar activities, cause cytotoxicity or inhibit the effect of drugs loaded onto the material. The present proof-of-concept study has confirmed the dual functioning of an approved drug as both a dispersant and a medication. The results of this work are expected to promote future research regarding the use of carbon-based nanomaterials in biomedicine and medicine.

Acknowledgments

This study was supported by a KAKENHI Grant-in-Aid for Scientific Research C (ID No. 17K11733 and ID No. 20K10025 to E. H) and KAKENHI Grant-in-Aid for Scientific Research B (ID No. 19H03839 to A. Y). Part of this work was conducted at Hokkaido University and supported by the “Nanotechnology Platform” Program of the Ministry of Education, Culture, Sports, Science, and Technology (MEXT), Japan. This study was also supported by JSPS Core-to-Core Program, A. Advanced Research Networks, and the Dynamic Alliance for Open Innovation Bridging Human, Environment and Materials.

References

[1] E. Miyako, T. Deguchi, Y. Nakajima, M. Yudasaka, Y. Hagihara, M. Horie, et al., Photothermic regulation of gene expression triggered by laser-induced carbon nanohorns, Proc. Natl. Acad. Sci. U. S. A. 109 (2012) 7523–7528.

[2] E. Miyako, K. Kono, E. Yuba, C. Hosokawa, H. Nagai, Y. Hagihara, Carbon nanotube–liposome supramolecular nanotrains for intelligent molecular-transport systems, Nat. Commun. 3 (2012) 1226.

[3] A. Battigelli, C. Ménard-Moyon, A. Bianco, Carbon nanomaterials as new tools for immunotherapeutic applications, J. Mater. Chem. B. 2 (2014) 6144–6156.

[4] A. Bianco, H.M. Cheng, T. Enoki, Y. Gogotsi, R.H. Hurt, N. Koratkar, et al., All in the graphene family - A recommended nomenclature for two-dimensional carbon materials, Carbon 65 (2013) 1–6.

[5] S.F. Oliveira, G. Bisker, N.A. Bakh, S.L. Gibbs, M.P. Landry, M.S. Strano, Protein functionalized carbon nanomaterials for biomedical applications, Carbon 95 (2015) 767–779.

[6] X. Cui, S. Xu, X. Wang, C. Chen, The nano-bio interaction and biomedical applications of carbon nanomaterials, Carbon 138 (2018) 436–450.

[7] B.P. Jiang, B. Zhou, Z. Lin, H. Liang, X.C. Shen, Recent advances in carbon nanomaterials for cancer phototherapy, Chem. - A Eur. J. 25 (2019) 3993–4004.

[8] M. Mamatha Kumari, D. Praveen Kumar, P. Haridoss, V. Durga Kumari, M.V. Shankar, Nanohybrid of titania/carbon nanotubes – nanohorns: A promising photocatalyst for enhanced hydrogen production under solar irradiation, Int. J. Hydrog. Energy 40 (2015) 1665–1674.

[9] P. Attri, J. Gaur, S. Choi, M. Kim, R. Bhatia, N. Kumar, et al., Interaction studies of carbon nanomaterials and plasma activated carbon nanomaterials solution with telomere binding protein, Sci. Rep. 7 (2017) 1–14.

[10] O.V. Kharissova, B.I. Kharisov, E.G. De Casas Ortiz, Dispersion of carbon nanotubes in water and non-aqueous solvents, RSC Adv. 3 (2013) 24812–24852.

[11] O.V. Kharissova, C.M. Oliva González, B.I. Kharisov, Solubilization and dispersion of carbon allotropes in water and non-aqueous solvents, Ind. Eng. Chem. Res. 57 (2018) 12624–12645.

[12] J. Texter, Graphene dispersions, Curr. Opin. Colloid Interface Sci. 19 (2014) 163–174.

[13] T. Fujigaya, N. Nakashima, Methodology for homogeneous dispersion of single-walled carbon nanotubes by physical modification, Polym. J. 40 (2008) 577-589.

[14] S. Iijima, M. Yudasaka, Nano-aggregates of single-walled graphitic carbon nano-horns, Chem. Phys. Lett. 309 (1999) 165–170.

[15] S. Lacotte, A. García, M. Décossas, W.T. Al-Jamal, S. Li, K. Kostarelos, S. Muller, et al., Interfacing functionalized carbon nanohorns with primary phagocytic cells, Adv. Mater. 20 (2008) 2421–2426.

[16] M. Zhang, M. Yang, C. Bussy, S. Iijima, K. Kostarelos, M. Yudasaka, Biodegradation of carbon nanohorns in macrophage cells, Nanoscale 7 (2015) 2834–2840.

[17] J. Miyawaki, M. Yudasaka, T. Azami, Y. Kubo, S. Iijima, Toxicity of single-walled carbon nanohorns, ACS Nano 2 (2008) 213–226.

[18] M. Vizuete, M.J. Gómez-Escalonilla, M. Barrejón, J.L.G. Fierro, M. Zhang, M. Yudasaka, et al., Synthesis, characterization and photoinduced charge separation of carbon nanohorn-oligothienylenevinylene hybrids, Phys. Chem. Chem. Phys. 18 (2016) 1828–1837.

[19] B. He, Y. Shi, Y. Liang, A. Yang, Z. Fan, L. Yuan, et al., Single-walled carbon-nanohorns improve biocompatibility over nanotubes by triggering less protein-initiated pyroptosis and apoptosis in macrophages, Nat. Commun. 9 (2018) 2393.

[20] T. Kasai, S. Matsumura, T. Iizuka, K. Shiba, T. Kanamori, M. Yudasaka, et al., Carbon nanohorns accelerate bone regeneration in rat calvarial bone defect, Nanotechnology 22 (2011) 065102.

[21] E. Hirata, E. Miyako, N. Hanagata, N. Ushijima, N. Sakaguchi, J. Russier, et al., Carbon nanohorns allow acceleration of osteoblast differentiation via macrophage activation, Nanoscale 8 (2016) 14514–14522.

[22] K. Ajima, M. Yudasaka, T. Murakami, A. Maigné, K. Shiba, S. Iijima, Carbon nanohorns as anticancer drug carriers, Mol. Pharm. 2 (2005) 475–480.

[23] N. Garrido-Mesa, A. Zarzuelo, J. Gálvez, Minocycline: Far beyond an antibiotic, Br. J. Pharmacol. 169 (2013) 337–352.

[24] K. Murata, K. Kaneko, W.A. Steele, F. Kokai, K. Takahashi, D. Kasuya, et al., Molecular potential structures of heat-treated single-wall carbon nanohorn assemblies, J. Phys. Chem. B. 105 (2001) 10210–10216.

[25] T. Murakami, K. Ajima, J. Miyawaki, M. Yudasaka, S. Iijima, K. Shiba, Drug-loaded carbon nanohorns: adsorption and release of dexamethasone in vitro, Mol. Pharm. 1 (2004) 399–405.

[26] J. Xu, M. Yudasaka, S. Kouraba, M. Sekido, Y. Yamamoto, S. Iijima, Single wall carbon nanohorn as a drug carrier for controlled release, Chem. Phys. Lett. 461 (2008) 189–192.

[27] T. Azami, D. Kasuya, R. Yuge, M. Yudasaka, S. Iijima, T. Yoshitake, et al., Large-scale production of single-wall carbon nanohorns with high purity, J. Phys. Chem. C. 112 (2008) 1330–1334.

[28] J. Fan, M. Yudasaka, D. Kasuya, T. Azami, R. Yuge, H. Imai, et al., Micrometer-sized graphitic balls produced together with single-wall carbon nanohorns, J. Phys. Chem. B. 109 (2005) 10756–10759.

[29] J. Fan, M. Yudasaka, J. Miyawaki, K. Ajima, K. Murata, S. Iijima, Control of hole opening in single-wall carbon nanotubes and single-wall carbon nanohorns using oxygen, J. Phys. Chem. B. 110 (2006) 1587–1591.

[30] M.J. Frisch, G.W. Trucks, H.B. Schlegel, G.E. Scuseria, M.A. Robb, J.R. Cheeseman, et al., Gaussian 09, Revision D.01, Gaussian Inc., Wallingford. (2013).

[31] A.D. Becke, Density-functional exchange-energy approximation with correct asymptotic behavior, Phys. Rev. A. 38 (1988) 3098-3100.

[32] C. Lee, W. Yang, R.G. Parr, Development of the Colle-Salvetti correlation-energy formula into a functional of the electron density, Phys. Rev. B. 37(1988) 785-789.

[33] M.M. Francl, W.J. Pietro, W.J. Hehre, J.S. Binkley, M.S. Gordon, D.J. DeFrees, et al., Self-consistent molecular orbital methods. XXIII. A polarization-type basis set for second-row elements, J. Chem. Phys. 77 (1982) 3654-3665.

[34] S. Grimme, J. Antony, S. Ehrlich, H. Krieg, A consistent and accurate ab initio parametrization of density functional dispersion correction (DFT-D) for the 94 elements H-Pu, J. Chem. Phys. 132 (2010) 154104.

[35] G.A. Petersson, A. Bennett, T.G. Tensfeldt, M.A. Al-Laham, W.A. Shirley, J. Mantzaris, A complete basis set model chemistry. I. The total energies of closed-shell atoms and hydrides of the first-row elements, J. Chem. Phys. 89 (1988) 2193-2218.

[36] G.A. Petersson, M.A. Al-Laham, A complete basis set model chemistry. II. Open-shell systems and the total energies of the first-row atoms, J. Chem. Phys. 94 (1991) 6081-6090.

[37] A. Nanci, S. Zalzal, Y. Gotoh, M.D. McKee, Ultrastructural characterization and immunolocalization of osteopontin in rat calvarial osteoblast primary cultures, Microsc. Res. Tech. 33 (1996) 214–231.

[38] Y. Takano, T. Numata, K. Fujishima, K. Miyake, K. Nakao, W.D. Grove, et al., Optical control of neuronal firing via photoinduced electron transfer in donor–acceptor conjugates, Chem. Sci. 7 (2016) 3331–3337.

[39] S. Chae, D. Kim, K.J. Lee, D. Lee, Y.O. Kim, Y.C. Jung, et al., Encapsulation and enhanced delivery of topoisomerase i inhibitors in functionalized carbon nanotubes, ACS Omega 3 (2018) 5938–5945.

[40] B.P. Jiang, L.F. Hu, X.C. Shen, S.C. Ji, Z. Shi, C.J. Liu, et al., One-step preparation of a water-soluble carbon nanohorn/phthalocyanine hybrid for dual-modality photothermal and photodynamic therapy, ACS Appl. Mater. Interfaces 6 (2014) 18008–18017.

[41] E. Bekyarova, K. Kaneko, M. Yudasaka, D. Kasuya, S. Iijima, A. Huidobro, et al., Controlled opening of single-wall carbon nanohorns by heat treatment in carbon dioxide, J. Phys. Chem. B. 107 (2003) 4479–4484.

[42] J.B. Park, Effects of doxycycline, minocycline, and tetracycline on cell proliferation, differentiation, and protein expression in osteoprecursor cells, J. Craniofac. Surg. 22 (2011) 1839–1842.

[43] Y. Tahara, J. Miyawaki, M. Zhang, M. Yang, I. Waga, S. Iijima, et al., Histological assessments for toxicity and functionalization-dependent biodistribution of carbon nanohorns, Nanotechnology 22 (2011) 265106.

[44] M. Zhang, D.A. Jasim, C. Ménard-Moyon, A. Nunes, S. Lijima, A. Bianco, et al., Radiolabeling, whole-body single photon emission computed tomography/computed tomography imaging, and pharmacokinetics of carbon nanohorns in mice, Int. J. Nanomedicine 11 (2016) 3317–3325.

[45] E. Hirata, M. Yudasaka, N. Ushijima, N. Sakaguchi, Y. Maeda, T. Tanaka, et al., Fate of carbon nanotubes locally implanted in mice evaluated by near-infrared fluorescence imaging: Implications for tissue regeneration, ACS Appl. Nano Mater. 2 (2019) 1382–1390.